

Super-quasicrystal stripe phases in optical superlattices with Raman-assisted tunneling

Junpeng Hou, Haiping Hu, Kuei Sun, and Chuanwei Zhang*

Department of Physics, The University of Texas at Dallas, Richardson, Texas 75080-3021, USA

Quasicrystal is a class of ordered structures defying conventional classification of solid crystals and may carry classically forbidden (e.g. 5-fold) rotational symmetries. In view of long-sought supersolids, a nature question is whether the quasicrystal order can also coexist with superfluidity, forming “super-quasicrystals”, which spontaneously break $U(1)$ symmetry due to superfluidity and forms quasicrystalline order that is not possessed by the underlying Hamiltonian. Here we show that a super-quasicrystal stripe state with the minimum 5-fold rotational symmetry can be realized as the ground state of a Bose-Einstein condensate in an optical superlattice with Raman-assisted tunneling. There exists a rich phase diagram consisting of various super-quasicrystal, supersolid, plane-wave phases, and their phase transitions. Our scheme can be generalized for generating other higher-order (e.g., 7-fold) quasicrystal states, and provides a platform for investigating such new exotic quantum matter.

Introduction. Quasicrystals exhibit exotic spatial patterns that are neither periodic as solid crystals (*i.e.*, lack of translational symmetry) nor totally disordered (*i.e.*, possession of long-range order) [1]. The Bragg diffraction peaks of quasicrystals possess rotational symmetries such as 5, 7, 8, 9, 10-fold that are forbidden in classical crystalline orders [1, 2]. Since its first report in Al-Mn and Al-Mn-Si alloys in 1984 [3], quasicrystal order has been studied and discovered in many different materials [4–9]. After years of dedicated study, icosahedrite, a newly-discovered mineral, confirmed the existence of natural quasicrystals [10].

Supersolid, another exotic phase of matter, combines solid crystalline structure with superfluidity, where two continuous symmetries, namely, translational and $U(1)$ gauge, are spontaneously broken [11]. Supersolids were first predicted for helium almost 50 years ago [12, 13], and recently have been observed in cold atom experiments [14, 15], where a strip phase with supersolid properties was generated and observed in a Bose-Einstein condensate (BEC) with superlattice denoted pseudospin states and associated spin-orbit coupling (SOC) [14]. These great advances in the study of supersolids raise a nature question: is it possible to create a novel quantum matter where both superfluidity and quasicrystal order coexist?

In this Letter, we address this question by proposing a scheme to generate a stable quasicrystal ground state in a BEC based on a practical generalization of the experimental setup for observing supersolid stripe phases [14, 16]. The experimental setup contains a 3D BEC confined in a 1D optical superlattice with quintuple well (define 5 pseudospin states), where neighboring wells are coupled by Raman assisted tunneling to generate an effective SOC. The scheme utilizes natural contact interaction and can realize quasicrystals with the minimum 5-fold rotational symmetry. In this quantum state, the $U(1)$ gauge symmetry is spontaneously broken just as that in supersolid stripe phases [14, 16]. However, the discrete translational symmetry, which is preserved

in supersolids, has also been broken, leaving only specified rotational symmetry. A quasicrystal order with such rotational symmetry is spontaneously formed although the underlying Hamiltonian does not possess such order. Therefore we denote this quantum matter as a ‘super-quasicrystal’. By tuning system parameters (e.g., Raman coupling strength, detuning, interaction, etc.), we show, through both variational ansatz analysis and direct simulation of mean field Gross-Pitaevskii equation (GPE), that there exists a rich phase diagram containing various super-quasicrystals, supersolids, and plane-wave phases. Our scheme can be further extended to generate any n -order super-quasicrystal phases, and should provide an excellent platform for exploring many interesting properties of super-quasicrystals, such as their quasiparticle excitations.

Experimental scheme and Hamiltonian. We consider a 3D BEC confined in a tilted superlattice potential

$$V_{SL}(z) = V_1 \sin^2(k_{L1}z) + V_2 \sin^2(k_{L2}z + \phi_{12}) + \alpha_z z \quad (1)$$

along the z -direction [Fig. 1(a)] with $k_{L2} = k_{L1}/5$. Here two lattices can come from the same laser source with the second lattice potential formed by two beams intersecting with an angle $\theta = 2 \arcsin(1/5)$. The linear potential $\alpha_z z$ can be realized with a magnetic field gradient. Note that this superlattice does not defy the definition for super-quasicrystal because it only breaks the translational symmetry in the z -direction, while the spontaneous formation of (quasi)crystal order is on the x - y plane. We denote five wells in each unit cell as five pseudospins and the effective couplings Ω between neighboring spins are induced by 5 Raman beams, one in the z direction and 4 in the x - y plane with designated wavevectors \hat{k}_j [Fig. 1(b)]. We choose suitable parameters ϕ_{12} , α_z such that the energy bias between neighboring wells $|\Delta_j| \gg J$ to avoid direct hopping (J is the bare tunneling rate without Raman coupling) and $||\Delta_j| - |\Delta_i|| \gg \Omega$ for $i \neq j$ so that two neighboring wells are coupled only by one specific Raman pair.

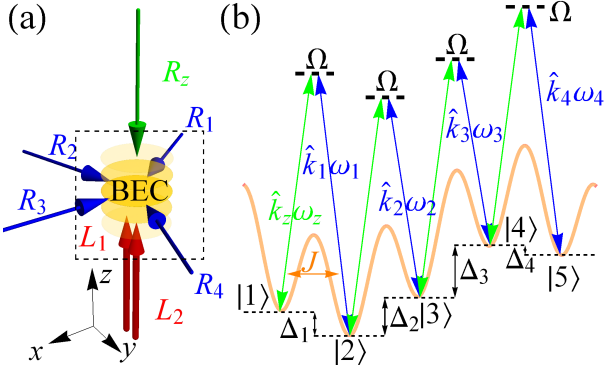


FIG. 1: (Color online) (a) Proposed experimental scheme for generating super-quasicrystals with 5-fold rotational symmetry. The superlattice is generated by two optical lattices with different periods. A potential gradient can be generated using a magnetic field gradient. One Raman beam R_z in the z -direction and four others ($R_j, j = 1, 2, 3, 4$) in the x - y plane generate the Raman coupling between neighboring wells. (b) SOC in one unit cell. Each Raman process only couples well j to its adjacent neighbor $j+1$. The hopping between neighboring unit cells is irrelevant because of the large bias between $|1\rangle$ and $|5\rangle$. Only Raman-assisted inter-well tunneling in a unit cell is considered.

The effective single particle Hamiltonian H_0 in the x - y plane can be written as

$$H_0 = \sum_{j=1}^5 \left[\frac{(\hat{p} - \hat{p}_j)^2}{2} + \delta_j \right] |j\rangle\langle j| + \sum_{j=1}^4 \left(\frac{\Omega}{2} |j\rangle\langle j+1| + h.c. \right), \quad (2)$$

after a standard unitary transformation of the pseudospin phases to remove the spatial dependence of the Raman coupling [17]. Here we choose the units as $\hbar = k_R = m = 1$, where k_R is recoil wavevector and m is atomic mass. The energy unit $E_R = \hbar^2 k_R^2 / m = 1$. δ_j is the detuning determined by the Raman transition. \hat{p}_j are the single particle band minima in momentum space without the Raman coupling satisfying $\hat{p}_j = \hat{p}_{j-1} + 2\hat{k}_{j-1}$ and $\hat{p}_1 = -\frac{2}{5} \sum_{j=1}^5 (5-j)\hat{k}_j$ [17]. In order to generate good super-quasicrystals, we consider a regular pentagon (all minima form an equilateral polygon) with $\hat{p}_1 = (0, 1)$, $\hat{p}_2 = (-\sqrt{5/8 + \sqrt{5}/8}, (-1 + \sqrt{5})/4)$, $\hat{p}_3 = (-\sqrt{5/8 - \sqrt{5}/8}, (-1 - \sqrt{5})/4)$, $\hat{p}_4 = (\sqrt{5/8 - \sqrt{5}/8}, (-1 - \sqrt{5})/4)$, and $\hat{p}_5 = (\sqrt{5/8 + \sqrt{5}/8}, (-1 + \sqrt{5})/4)$ [see Fig. 2(a)], which can be realized using $\hat{k}_j = (\hat{p}_{j+1} - \hat{p}_j)/2$ ($j = 1, 2, 3, 4$) for four Raman lasers in the xy plane.

For $\Omega = 0$ and $\delta_j = 0$ [Fig. 2(a)], five minima distribute over the vertexes of a regular pentagon. All spin components are uncoupled and only occupy one minimum. As a strong Raman coupling $\Omega = 0.4$ is ramped on [Fig. 2(b)], the minima are coupled as an open boundary

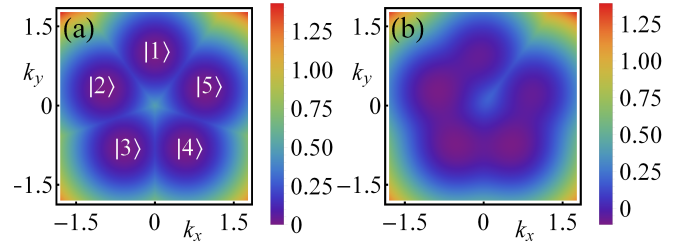


FIG. 2: (Color online) Single particle lowest band dispersion. (a) $\Omega = 0$. the minima form a regular pentagon structure in the momentum space. (b) $\Omega = 0.4$. The minima are strongly coupled and all spin component are mixed. Wells 1 and 5 are uncoupled and a barrier between them can be observed. The five minima are axisymmetric to \hat{p}_3 for any Ω .

chain without coupling between head and tail. The spin components are mixed at each minimum and each well starts to merge with its adjacent neighbor. Because the locations of all minima [labelled as in Fig. 2(a)] are axisymmetric to the vector \hat{p}_3 , the two uncoupled minima (the head and the tail) disappear first at certain critical value of Ω (we label the remaining minima as 2 to 4). Finally, the remaining three minima merge into one (minimum 3) approximately located at $(-0.207, -0.286)$ [17] when Ω is extremely strong and its location is still along the same line as \hat{p}_3 .

Phase diagram. We now study new quantum phases emerging from interactions between atoms, which can be described by the GPE under the mean-field approximation with energy density

$$\epsilon = \int \frac{d\hat{r}}{V} \left[\psi^\dagger H_0 \psi + \frac{c_0}{2} n_i^2 + \frac{c_2}{2} \sum_{i=1}^4 n_i n_{i+1} \right], \quad (3)$$

where ψ is the 5-component spinor wavefunction, $n_i = \psi_i^\dagger \psi_i$ is the density for the spin component i , c_0 and $c_2 \approx \frac{J}{\Delta} c_0$ are density interaction for the same and neighboring spins, respectively. For realistic parameters, $J/\Delta \sim 1/20$, the neighboring spin interaction can be ignored [14] and this is a crucial condition for realizing super-quasicrystals or supersolids in experiments. The wavefunction is normalized by the average atomic density as $V^{-1} \int d\hat{r} \psi^\dagger \psi = \bar{n}$ with V being the system volume. We obtain the ground state using both variational ansatz analysis and direct numerical simulation of the GPE, and they agree well.

The general form of the variational ansatz is

$$\psi = \sqrt{\bar{n}} \sum_{j=1}^5 C_j e^{i\hat{k}_{m,j} \cdot \hat{r}} \xi_j, \quad (4)$$

where C_j are complex numbers satisfying normalization relation $\sum_j |C_j|^2 = 1$, $\hat{k}_{m,j}$ denotes each minimum in momentum space and ξ_j are the spinor part of wavefunction $\xi_j = (\cos \alpha_j \cos \beta_j \cos \gamma_j, \cos \alpha_j \cos \beta_j \sin \gamma_j, \sin \alpha_j, \cos \alpha_j \sin \beta_j \sin \gamma_j, \cos \alpha_j \sin \beta_j \cos \gamma_j)^T$. We assume

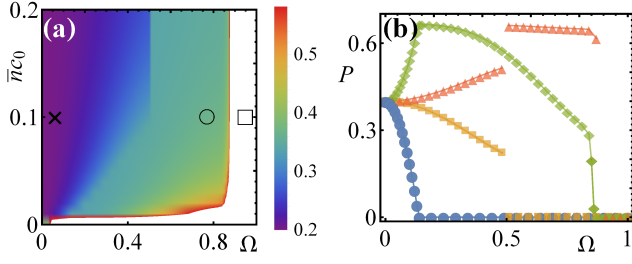


FIG. 3: (Color online) (a) Phase diagram from the variational ansatz analysis when all the detunings are set to be zero. The color represents the value of $|C_3|^2$. The white region is the plane-wave phase. The three symbols (cross, circle, and square stand for $\Omega = 0.06, 0.77$ and 0.95) along $\bar{n}c_0 = 0.1$ are examples for super-quasicrystal, supersolid, and plane-wave phases. (b) Phase transitions between different phases. The blue circles (green rhombus) and orange squares (red triangles) show how $|C_1|^2 + |C_5|^2$ ($|C_2|^2 + |C_4|^2$) varies with Raman coupling for $\bar{n}c_0 = 0.01$ and 0.2 , respectively.

$\xi_{1,j} = \xi_{5,6-j}$, $\xi_{2,j} = \xi_{4,6-j}$ ($\xi_{i,j}$ stands for the j th component of spinor ξ_i), and $\hat{k}_{m,1}(\hat{k}_{m,2})$ and $\hat{k}_{m,5}(\hat{k}_{m,4})$ are axisymmetric to vector $\hat{k}_{m,3}$ based on the symmetry of the Hamiltonian. Generally it is challenging to optimize the energy density functional with so many variables. However, in the weak interaction region $\bar{n}c_0 \ll 1$, the BEC wavefunction at each band minimum is quite close to the single particle spinor wavefunction, which can thus be used to fix ξ_j for the variational calculation. Similar method was used previously for studying spin-1 spin-orbit coupled BEC, which gives all phases as those in full variational calculation, although the phase boundary may be slightly different for stronger interaction [18]. We also find that $C_1 = C_5$ and $C_2 = C_4$ hold in weak interaction situations.

In Fig. 3(a), we plot the phase diagram with respect to the interaction strength $\bar{n}c_0$ and Raman coupling strength Ω obtained from the variational ansatz calculation, where the color shows the occupied probability $|C_3|^2$ at the momentum minimum 3. At a finite Ω , 3 has the lowest energy, therefore atoms only occupy 3 without interaction, leading to a plane-wave phase. On the other hand, a strong density-density interaction prefers the equal occupation of all minima. Therefore the competition between Raman coupling and interaction may render different phases, as shown in Fig. 3(a).

In the small Ω region, all five minima are equally populated with the same probability $1/5$ due to interaction, forming a super-quasicrystal [cross in 3(a)]. This new quantum matter is confirmed by the real and momentum space density distributions [Fig. 4(a,b)] obtained from the GPE simulation in a harmonic trap. We see the distribution in the real space is indeed in lack of translational symmetry, while in momentum space five equally populated peaks form a regular pentagon with each vertex designated as \hat{p}_j , showing the 5-fold rotational symmetry

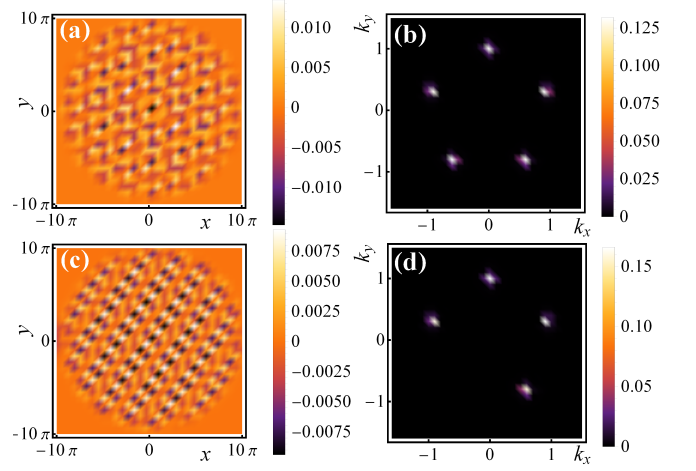


FIG. 4: (Color online) (a)[(b)] Real-space (momentum-space) distribution for the super-quasicrystal phase from GPE simulation. The parameters are the same as the black cross marked in Fig. 3(a). The five minima in momentum space are evenly populated. (c)[(d)] Real-space (momentum-space) distribution for a supersolid phase when one minimum is knocked off with a small detuning $\delta_3 \sim 0.01E_R$ in the super-quasicrystal phase in (a,b). All real-space density distributions (including following panels) are obtained through subtracting the real-space density at zero Raman coupling from those of finite Ω to rule out the large density variation across the harmonic trap. The plots are rescaled over the average density in the trap. The total momentum-space distribution is the direct summation of that for each spin component.

of the super-quasicrystal phase.

With the increase in Ω , the occupation of five minima changes to three, leading to a supersolid stripe phase [circle in Fig. 3(a)], where $|C_3|^2$ increases to ~ 0.35 . The resulting real and momentum space density distributions from GPE are shown in Fig. 5(a). Here a clear translational symmetry in the real space is observed. In the momentum space distribution (bottom inset), three minima are occupied unevenly and minimum 3 has a larger weight. Here Ω is quite large and the spin components in each minimum are mixed. Consequently, the spatial distribution of state $|3\rangle$ exhibits clear density modulation (top inset). For a very large Ω , all minima merge to one and the system enters a plane-wave phase [square in 3(a)]. In Fig. 5(b), we plot its phase distribution obtained from GPE, which shows a stripe pattern as expected. The overall real space density distribution (top inset) is a Gaussian-type wavepacket and the BEC occupies one point in the momentum space (bottom inset).

We characterize the transition between these phases in Fig. 3(b), where we plot the populations $P_{15} = |C_1|^2 + |C_5|^2$ and $P_{24} = |C_2|^2 + |C_4|^2$ with respect to Ω for two different interaction strengths $\bar{n}c_0 = 0.01$ and 0.2 . In the weak interaction case $\bar{n}c_0 = 0.01$, P_{15} smoothly decreases to 0 and P_{24} has a sharp turn at certain Ω , showing a second-order phase transition from super-quasicrystal to

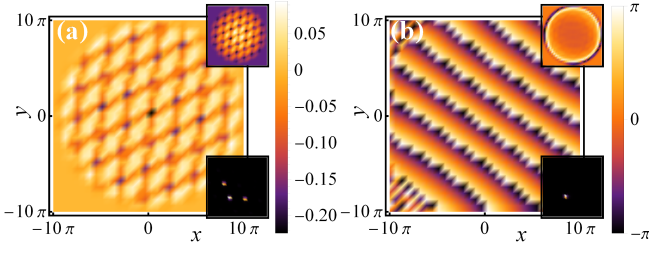


FIG. 5: (Color online) (a) Spatial distribution for a supersolid phase [parameters chosen as black circle in Fig. 3(a)] with three minima populated. The top and bottom insets show the real-space density of state $|3\rangle$ and the momentum-space distribution respectively. (b) Phase distribution for state $|3\rangle$ at a nonzero momentum plane-wave phase and the insets give real (top) and momentum (bottom) space distributions. The parameters correspond to the black square in Fig. 3(a).

supersolids. This occurs when the energy bias between minima 1 and 2 with increasing Ω is larger than the interaction energy cost. For the strong interaction $\bar{n}c_0 = 0.2$, P_{15} (P_{24}) shows a sudden drop at $\Omega \sim 0.5$, showing a first-order phase transition at the point where single particle five minima merge into three. Before the transition, the interaction energy cost is so strong that P_{15} is always nonzero. Around $\Omega \sim 0.8$, the three minima merge into one and P_{24} also suddenly drops to zero, showing a second order phase transition to the plane wave phase.

In addition to varying Ω , we may also adjust detuning δ_j to change the relative population of the minima. In Fig. 4(c,d), we plot the real and momentum-space distribution from GPE by adding a small detuning $\delta_3 \sim 0.01E_R$ in spin state $|3\rangle$ for the super-quasicrystal state in Fig 4(a). We see that the minimum 3 is now knocked out and the translational symmetry is restored. The BEC becomes a supersolid with exotic real-space distribution because it is still populated on four of five vertexes of a regular pentagon. The interplay among Raman coupling, detuning, and interaction leads to a rich phase diagram and hence enables the designing and engineering of new super-quasicrystal and supersolid phases.

Experimental realization and detection. The experimental realization of our scheme is based on recent experimental reports on observing supersolid stripe phases [14, 16]. Consider $N = 10^5$ ^{23}Na atoms confined in a super-lattice with five wells in one unit cell and the condensate is initially split into each well equally with an average density around $\bar{n} = 0.5 \times 10^{14} \text{ cm}^{-3}$. We choose $k_R = 1064 \text{ nm}$ and $E_R = 7672 \text{ Hz}$ for Raman lasers. The Raman coupling strength Ω can be tuned as low as 300 Hz [14, 16], that is, $\Omega \lesssim 0.08E_R$, which well resides in the super-quasicrystal region. In real experiments, $(c_0 - c_2)/c_0 \approx 1$, therefore the neighboring-spin interaction term can be neglected. The same spin density interaction strength can be evaluated with $c_0 = 4\pi\hbar^2 a_s/m$, where a_s is the two-body scattering length. Taking $a_s =$

$50a_0$ (a_0 is Bohr radius) [19, 20], we have $\bar{n}c_0 \approx 0.1E_R$, which is sufficiently strong for the observation of super-quasicrystals although a larger density \bar{n} yields a larger parameter region (Fig. 3) and is better for the observation of super-quasicrystal phases.

In experiments, the super-quasicrystal phases may be observed in the time-of-flight (TOF) image, where five equally populated peaks are formed in the momentum space at designated positions [Fig. 4(b)]. By measuring P_{15} and P_{24} in TOF, the quantum phase transition between different phases in Fig. 3(b) can be detected. Another way to observe the super-quasicrystal phases is using Bragg scattering, similar to that for supersolids [14], where the Bragg diffraction patterns for super-quasicrystals should give peaks possessing 5-fold rotational symmetry [2].

Discussion and Conclusion. Our proposed experimental setup can be straightforwardly generalized for realizing other super-quasicrystal phases with higher order rotational symmetry, such as $n = 7$, where 7 Raman lasers are needed with a similar experimental setup for 7 wells in a superlattice. Similar idea can also be applied to a spin-orbit coupled BEC with the hyperfine state pseudospins [21–33] to generate super-quasicrystal phases. In a spin-orbit coupled BEC, supersolid stripe phases have been proposed [34–44] for both 1D and 2D SOC, but not yet observed in experiments. Note that our proposed scheme for super-quasicrystals requires five almost degenerate band minima for five different spins to generate a regular pentagon in the momentum space. In experiments, an effective 2D SOC (not exactly Rashba) has been experimentally realized recently [31–33] by coupling three spin states at three degenerate band minima, although the resulting band minimum path in the lowest band is not a flat ring as expected from a Rashba SOC. In our scheme, no flat Rashba ring is needed and 5 Raman lasers with suitable wavevectors and polarizations are chosen such that the effective band minima are formed at \hat{p}_j for a regular pentagon. The crucial difficulty comes from the interaction that is almost isotropic between any spin states. This difficulty may be resolved using ^{133}Cs atoms [45], where the interaction may be tuned by Feshbach resonance to favor the equal occupation of five minima in the momentum space, instead of the plane-wave at one minimum.

In summary, we have proposed a scheme for realizing super-quasicrystal stripe phases using a BEC in a 1D quintuple-well optical superlattices with Raman-assisted tunneling, which is a practical generalization of the experimental setup for recent observation of supersolid stripe phases. Through variational and GPE analysis, we show there is a rich phase diagram containing super-quasicrystals, supersolids, plane-wave phases, and their phase transitions. Our proposed experimental setup should lay out a platform for future theoretical and experimental investigations of such exotic novel quantum

matter.

Acknowledgments: This work is supported by AFOSR (FA9550-16-1-0387), NSF (PHY-1505496), and ARO (W911NF-17-1-0128).

* Corresponding author.

Email: chuanwei.zhang@utdallas.edu

- [1] J. Christian, Neutron and Synchrotron Radiation for Condensed Matter Studies, Springer Berlin Heidelberg, 1994.
- [2] D. Levine and P. J. Steinhardt, Quasicrystals: A New Class of Ordered Structures, *Phys. Rev. Lett.* **53**, 2477 (1984).
- [3] D. Shechtman, I. Blech, D. Gratias, and J. W. Cahn, Metallic Phase with Long-Range Orientational Order and No Translational Symmetry, *Phys. Rev. Lett.* **53**, 1951 (1984).
- [4] E. Maciá, The role of aperiodic order in science and technology, *Rep. Prog. Phys.* **69**, 397 (2006).
- [5] B. Freedman, R. Lifshitz, J. W. Fleischer & M. Segev, Phason dynamics in nonlinear photonic quasicrystals, *Nat. Mater.* **6**, 776 (2007).
- [6] K. Barkan, H. Diamant, and R. Lifshitz, Stability of quasicrystals composed of soft isotropic particles, *Phys. Rev. B* **83**, 172201 (2011).
- [7] N. A. Wasio, R. C. Quardokus, R. P. Forrest, C. S. Lent, S. A. Corcelli, J. A. Christie, K. W. Henderson & S. Alex Kandel, Self-assembly of hydrogen-bonded two-dimensional quasicrystals, *Nature (London)* **507**, 86 (2014).
- [8] K. Nagao, T. Inuzuka, K. Nishimoto, and K. Edagawa, Experimental Observation of Quasicrystal Growth, *Phys. Rev. Lett.* **115**, 075501 (2015).
- [9] J. I. Urgel, D. Écija, G. Lyu, R. Zhang, C.-A. Palma, W. Auwärter, N. Lin & J. V. Barth, Quasicrystallinity expressed in two-dimensional coordination networks, *Nat. Chem.* **8**, 657 (2016).
- [10] L. Bindi, P. J. Steinhardt, N. Yao, P. J. Lu, Natural Quasicrystals, *Science* **324**, 1306 (2009).
- [11] M. Boninsegni and N. V. Prokofv, Supersolids: What and where are they? *Rev. Mod. Phys.* **84**, 759 (2012).
- [12] D.J. Thouless, The flow of a dense superfluid, *Ann. Phys.* **52**, 403 (1971).
- [13] A. F. Andreev and I. M. Lifshitz, Quantum Theory of Defects in Crystals, *Sov. Phys. JETP* **29**, 1107 (1971).
- [14] J.-R. Li, J. Lee, W. Huang, S. Burchesky, B. Shteynas, F. Ç. Top, A. O. Jamison, and W. Ketterle, A stripe phase with supersolid properties in spin-orbit-coupled Bose-Einstein condensates, *Nature (London)* **543**, 91 (2017).
- [15] J. Léonard, A. Morales, P. Zupancic, T. Esslinger & T. Donner, Supersolid formation in a quantum gas breaking a continuous translational symmetry, *Nature (London)* **543**, 87 (2017).
- [16] J. Li, W. Huang, B. Shteynas, S. Burchesky, F. Top, E. Su, J. Lee, A. O. Jamison, and W. Ketterle, Spin-Orbit Coupling and Spin Textures in Optical Superlattices, *Phys. Rev. Lett.* **117**, 185301 (2016).
- [17] Supplementary materials, see supplementary materials for details.
- [18] X.-W. Luo, K. Sun, C. Zhang, Spin-tensor-momentum-coupled Bose-Einstein condensates, [arXiv:1705.03920](https://arxiv.org/abs/1705.03920).
- [19] F. A. van Abeelen and B. J. Verhaar, Determination of collisional properties of cold Na atoms from analysis of bound-state photoassociation and Feshbach resonance field data, *Phys. Rev. A* **59**, 578 (1999).
- [20] S. Knoop, T. Schuster, R. Scelle, A. Trautmann, J. Appmeier, M. K. Oberthaler, E. Tiesinga, and E. Tiemann, Feshbach spectroscopy and analysis of the interaction potentials of ultracold sodium, *Phys. Rev. A* **83**, 042704 (2011).
- [21] Y.-J. Lin, K. Jiménez-García, and I. B. Spielman, Spin-orbit-coupled Bose-Einstein condensates, *Nature (London)* **471**, 83 (2011).
- [22] J.-Y. Zhang, S.-C. Ji, Z. Chen, L. Zhang, Z.-D. Du, B. Yan, G.-S. Pan, B. Zhao, Y.-J. Deng, H. Zhai, S. Chen, and J.-W. Pan, Collective Dipole Oscillations of a Spin-Orbit Coupled Bose-Einstein Condensate, *Phys. Rev. Lett.* **109**, 115301 (2012).
- [23] C. Qu, C. Hamner, M. Gong, C. Zhang, and P. Engels, Observation of Zitterbewegung in a spin-orbit-coupled Bose-Einstein condensate, *Phys. Rev. A* **88**, 021604(R) (2013).
- [24] A. J. Olson, S.-J. Wang, R. J. Niffenegger, C.-H. Li, C. H. Greene, and Y. P. Chen, Tunable Landau-Zener transitions in a spin-orbit-coupled Bose-Einstein condensate, *Phys. Rev. A* **90**, 013616 (2014).
- [25] C. Hamner, C. Qu, Y. Zhang, J. Chang, M. Gong, C. Zhang, and P. Engels, Dicke-type phase transition in a spin-orbit-coupled Bose-Einstein condensate, *Nat. Commun.* **5**, 4023 (2014).
- [26] P. Wang, Z.-Q. Yu, Z. Fu, J. Miao, L. Huang, S. Chai, H. Zhai, and J. Zhang, Spin-Orbit Coupled Degenerate Fermi Gases, *Phys. Rev. Lett.* **109**, 095301 (2012).
- [27] L. W. Cheuk, A. T. Sommer, Z. Hadzibabic, T. Yefsah, W. S. Bakr, and M. W. Zwierlein, Spin-Injection Spectroscopy of a Spin-Orbit Coupled Fermi Gas, *Phys. Rev. Lett.* **109**, 095302 (2012).
- [28] R. A. Williams, M. C. Beeler, L. J. LeBlanc, K. Jiménez-García, and I. B. Spielman, Raman-Induced Interactions in a Single-Component Fermi Gas Near an s-Wave Feshbach Resonance, *Phys. Rev. Lett.* **111**, 095301 (2013).
- [29] N. Q. Burdick, Y. Tang, and B. L. Lev, Long-Lived Spin-Orbit-Coupled Degenerate Dipolar Fermi Gas, *Phys. Rev. X* **6**, 031022 (2016).
- [30] B. Song, C. He, S. Zhang, E. Hagiye, W. Huang, X.-J. Liu, and G.-B. Jo, Spin-orbit-coupled two-electron Fermi gases of ytterbium atoms, *Phys. Rev. A* **94**, 061604(R) (2016).
- [31] L. Huang, Z. Meng, P. Wang, P. Peng, S.-L. Zhang, L. Chen, D. Li, Q. Zhou & J. Zhang, Experimental realization of two-dimensional synthetic spin-orbit coupling in ultracold Fermi gases, *Nat. Phys.* **12**, 540 (2016).
- [32] Z. Meng, L. Huang, P. Peng, D. Li, L. Chen, Y. Xu, C. Zhang, P. Wang, and J. Zhang, Experimental Observation of a Topological Band Gap Opening in Ultracold Fermi Gases with Two-Dimensional Spin-Orbit Coupling, *Phys. Rev. Lett.* **117**, 235304 (2016).
- [33] Z. Wu, L. Zhang, W. Sun, X.-T. Xu, B.-Z. Wang, S.-C. Ji, Y. Deng, S. Chen, X.-J. Liu, J.-W. Pan, Realization of two-dimensional spin-orbit coupling for Bose-Einstein condensates, *Science* **354**, 83 (2016).
- [34] T. D. Stanescu, B. Anderson, and V. Galitski, Spin-orbit coupled Bose-Einstein condensates, *Phys. Rev. A* **78**, 023616 (2008).

- [35] C. Wu, I. Mondragon-Shem, and X.-F. Zhou, Unconventional Bose-Einstein Condensations from Spin-Orbit Coupling, *Chin. Phys. Lett.* **28**, 097102 (2011).
- [36] C. Wang, C. Gao, C.-M. Jian, and H. Zhai, Spin-orbit coupled spinor Bose-Einstein condensates, *Phys. Rev. Lett.* **105**, 160403 (2010).
- [37] T.-L. Ho and S. Zhang, Bose-Einstein condensates with spin-orbit interaction, *Phys. Rev. Lett.* **107**, 150403 (2011).
- [38] Y. Li, L. Pitaevskii, and S. Stringari, Quantum tricriticality and phase transitions in spin-orbit coupled Bose-Einstein condensates, *Phys. Rev. Lett.* **108**, 225301 (2012).
- [39] Y. Zhang, L. Mao, and C. Zhang, Mean-field dynamics of spin-orbit coupled Bose-Einstein condensates, *Phys. Rev. Lett.* **108**, 035302 (2012).
- [40] H. Hu, B. Ramachandhran, H. Pu, and X.-J. Liu, Spin-orbit coupled weakly interacting Bose-Einstein condensates in harmonic traps, *Phys. Rev. Lett.* **108**, 010402 (2012).
- [41] T. Ozawa and G. Baym, Stability of ultracold atomic bose condensates with rashba spin-orbit coupling against quantum and thermal fluctuations, *Phys. Rev. Lett.* **109**, 025301 (2012).
- [42] K. Sun, C. Qu, Y. Xu, Y. Zhang, and C. Zhang, Interacting spin-orbit-coupled spin-1 Bose-Einstein condensates, *Phys. Rev. A* **93**, 023615 (2016).
- [43] Z.-Q. Yu, Phase transitions and elementary excitations in spin-1 Bose gases with Raman-induced spin-orbit coupling, *Phys. Rev. A* **93**, 033648 (2016).
- [44] G. Martone, F. Pepe, P. Facchi, S. Pascazio, and S. Stringari, Tricriticalities and quantum phases in spin-orbit-coupled spin-1 bose gases, *Phys. Rev. Lett.* **117**, 125301 (2016).
- [45] L. W. Clark, L.-C. Ha, C.-Y. Xu, and C. Chin, Quantum Dynamics with Spatiotemporal Control of Interactions in a Stable Bose-Einstein Condensate, *Phys. Rev. Lett.* **115**, 155301 (2015).

Supplementary materials

Single particle Hamiltonian for spin-orbit-coupling

Here, we derive the effective Hamiltonian for our pseudospin system with $n = 5$ and the results can be readily generalized to arbitrary n situation. Results for the $n = 2$ case have been studied with great details in [16]. The initial Hamiltonian for the whole system consists of two parts, the superlattice V_{SL} in the z -direction as well as the Raman coupling. We first consider the superlattice potential with a tilted potential

$$H_{SL} = \frac{\hat{p}^2}{2} + \frac{p_z^2}{2} + V_1 \sin^2(k_{L1}z) + V_2 \sin^2(k_{L2}z + \phi_{12}) + \alpha_z z. \quad (5)$$

It can be rewritten in the tight-binding approximation as

$$\begin{aligned} H_{SL} = & \frac{\hat{p}^2}{2} + \Delta_1 \sum_m (|\Psi_{1,m}\rangle\langle\Psi_{1,m}|) + \Delta_2 \sum_m (|\Psi_{1,m}\rangle\langle\Psi_{1,m}| + |\Psi_{2,m}\rangle\langle\Psi_{2,m}|) \\ & - \Delta_4 \sum_m (|\Psi_{5,m}\rangle\langle\Psi_{5,m}|) - \Delta_3 \sum_m (|\Psi_{4,m}\rangle\langle\Psi_{4,m}| + |\Psi_{5,m}\rangle\langle\Psi_{5,m}|) \\ & + J \sum_m \sum_{i=1}^4 (|\Psi_{i,m}\rangle\langle\Psi_{i+1,m}| + h.c.) + \sum_m \sum_{i=1}^5 \sum_{j=1}^5 (J_{i,j} |\Psi_{i,m}\rangle\langle\Psi_{j,m+1}| + h.c.), \end{aligned} \quad (6)$$

where $|\Psi_{i,m}\rangle$ is the onsite wavefunction of well j in the m -th unit cell. We have set well 3 to be the reference of zero-energy and define the difference Δ_j to be the height of well j minus that of well $j+1$. In the following, we neglect the coupling $J_{i,j}$ between adjacent unit cell because there is no Raman assisted tunneling between wells in different unit cells. The four Raman couplings are

$$V_{Raman,j} = \Omega_j \cos(k_z z + \hat{k}_j \cdot \hat{r} - \delta_{R,j} t). \quad (7)$$

Since $J \ll \Delta_j$, we consider only the first-order perturbation so that the wavefunctions are

$$\begin{aligned} |1, m\rangle &= |\Psi_{1,m}\rangle + \frac{J}{\Delta_1} |\Psi_{2,m}\rangle, \quad |2, m\rangle = |\Psi_{2,m}\rangle - \frac{J}{\Delta_1} |\Psi_{1,m}\rangle + \frac{J}{\Delta_2} |\Psi_{3,m}\rangle, \\ |3, m\rangle &= |\Psi_{3,m}\rangle - \frac{J}{\Delta_2} |\Psi_{2,m}\rangle + \frac{J}{\Delta_3} |\Psi_{4,m}\rangle, \quad |4, m\rangle = |\Psi_{4,m}\rangle - \frac{J}{\Delta_3} |\Psi_{3,m}\rangle + \frac{J}{\Delta_4} |\Psi_{5,m}\rangle, \\ |5, m\rangle &= |\Psi_{5,m}\rangle - \frac{J}{\Delta_4} |\Psi_{4,m}\rangle, \end{aligned} \quad (8)$$

and the energy separations are unchanged. Now, we may expand H_{SL} in the basis after perturbation

$$\begin{aligned} H_{SL} = & \frac{\hat{p}^2}{2} + \Delta_1 \sum_m (|1, m\rangle\langle 1, m|) + \Delta_2 \sum_m (|1, m\rangle\langle 1, m| + |2, m\rangle\langle 2, m|) \\ & - \Delta_4 \sum_m (|5, m\rangle\langle 5, m|) - \Delta_3 \sum_m (|4, m\rangle\langle 4, m| + |5, m\rangle\langle 5, m|) \\ & + \sum_{\hat{p}, \hat{p}'} |\hat{p}\rangle \left(\sum_{n'} \sum_{i=1}^5 \sum_{j=1}^5 |i, m\rangle\langle i, m| \langle \hat{p} | \Omega_j \cos(k_z z + \hat{k}_j \cdot \hat{r} - \delta_{R,j} t) | \hat{p}' \rangle |j, m\rangle\langle j, m| \right) \langle \hat{p}' | \end{aligned} \quad (9)$$

Assume d is the period of the superlattice, we then require $k_{L1} \sim \pi/d$, $k_{L2} \sim 5\pi/d$ and $k_z \sim 5\pi/(2d)$. Now, we turn to estimating the overlap integrals for $\cos(k_z(z - z_m))$ and $\sin(k_z(z - z_m))$ to the first order in J/Δ_j

$$\begin{aligned} \langle 1, m | \cos(k_z(z - z_m)) | 2, m \rangle &= -\frac{J}{\Delta_1}, \quad \langle 2, m | \cos(k_z(z - z_m)) | 3, m \rangle = -\frac{J}{\Delta_2}, \\ \langle 3, m | \cos(k_z(z - z_m)) | 4, m \rangle &= \frac{J}{\Delta_3}, \quad \langle 4, m | \cos(k_z(z - z_m)) | 5, m \rangle = \frac{J}{\Delta_4}, \\ \langle 1, m | \sin(k_z(z - z_m)) | 2, m \rangle &= \frac{J}{\Delta_1}, \quad \langle 2, m | \sin(k_z(z - z_m)) | 3, m \rangle = -\frac{J}{\Delta_2}, \\ \langle 3, m | \sin(k_z(z - z_m)) | 4, m \rangle &= -\frac{J}{\Delta_3}, \quad \langle 4, m | \sin(k_z(z - z_m)) | 5, m \rangle = \frac{J}{\Delta_4}, \\ \langle j, m | \cos(k_z(z - z_m)) | j, m \rangle &= \sin(\frac{\pi}{2}j), \quad \langle j, m | \sin(k_z(z - z_m)) | j, m \rangle = -\cos(\frac{\pi}{2}j), \end{aligned} \quad (10)$$

where $z_m = md$ gives the position of the 1st well in the m th unit cell. With those relations, we can reformulate Raman potential as

$$\begin{aligned}
& \sum_{i=1}^5 \sum_{j=1}^5 |i, m\rangle \langle i, m| \langle \hat{p} | \Omega \cos(k_z z + \hat{k}_j \cdot \hat{r} - \delta_j t) | \hat{p}' \rangle |j, m\rangle \langle j, m| \\
&= \Omega_j \cos \phi_{m,j} (|1, m\rangle \langle 1, m| - |3, m\rangle \langle 3, m| + |5, m\rangle \langle 5, m|) \\
&+ \Omega_j \cos \phi_{m,j} \left(-\frac{J}{\Delta_1} |1, m\rangle \langle 2, m| - \frac{J}{\Delta_2} |2, m\rangle \langle 3, m| + \frac{J}{\Delta_3} |3, m\rangle \langle 4, m| + \frac{J}{\Delta_4} |4, m\rangle \langle 5, m| \right) \\
&+ \Omega_j \sin \phi_{m,j} (|2, m\rangle \langle 2, m| - |4, m\rangle \langle 4, m|) \\
&+ \Omega_j \sin \phi_{m,j} \left(\frac{J}{\Delta_1} |1, m\rangle \langle 2, m| - \frac{J}{\Delta_2} |2, m\rangle \langle 3, m| - \frac{J}{\Delta_3} |3, m\rangle \langle 4, m| + \frac{J}{\Delta_4} |4, m\rangle \langle 5, m| \right),
\end{aligned} \tag{11}$$

where $\phi_{m,j} = \pi m/2 + \hat{k}_j \cdot \hat{r} - \delta_{R,j} t$. We adjust each $\delta_{R,j}$ close to Δ_j and require that it is off-resonate to other $\Delta_i, i \neq j$ so that the Raman potential $V_{Raman,j}$ only couples $|j, m\rangle$ to its neighbor state $|j+1, m\rangle$. Initially, we assume all the atoms are prepared in well j , which is the state with $q = (j-1)2\pi/(5d)$ of the lowest band of the superlattice

$$|\psi_{q=(j-1)2\pi/(5d)}^{(j)}\rangle = \sum_{m=1}^N \frac{1}{\sqrt{N}} e^{i \frac{2\pi(j-1)}{5d} [z_m + (j-1)\frac{d}{5}]} |j, m\rangle. \tag{12}$$

Here N is the number of all unit cell in the superlattice. For its adjacent well $j+1$, the lowest state is

$$|\psi_{q=j2\pi/(5d)}^{(j+1)}\rangle = \sum_{m=1}^N \frac{1}{\sqrt{N}} e^{i \frac{2\pi j}{5d} (z_m + j\frac{d}{5})} |j+1, m\rangle. \tag{13}$$

Note that, from here to the end of this section, i is the imaginary unit unless otherwise specified. We first calculate the intra-band couplings

$$\langle \psi_{q=j2\pi/(5d)}^{(j)} | V_{Raman,j} | \psi_{q=(j-1)2\pi/(5d)}^{(j)} \rangle = \sum_{m,m'} \frac{1}{N} e^{i \frac{2\pi}{5} [(m'-m-\frac{1}{5})j - m' + \frac{1}{5}]} \langle j, m | V_{Raman,j} | j, m' \rangle \tag{14}$$

$$= \sum_m \frac{1}{N} e^{-i \frac{2\pi}{5} [m + (j-1)\frac{1}{5}]} \langle j, m | V_{Raman,j} | j, m \rangle,$$

$$\langle \psi_{q=(j-1)2\pi/(5d)}^{(j+1)} | V_{Raman,j} | \psi_{q=j2\pi/(5d)}^{(j+1)} \rangle = \sum_{m,m'} \frac{1}{N} e^{i \frac{2\pi}{5} [(m'-m-\frac{1}{5})j - m]} \langle j+1, m | V_{Raman,j} | j+1, m' \rangle \tag{15}$$

$$= \sum_m \frac{1}{N} e^{-i \frac{2\pi}{5} [m - \frac{j}{5}]} \langle j+1, m | V_{Raman,j} | j+1, m \rangle,$$

and then, the SOC terms

$$\begin{aligned}
\langle \psi_{q=j2\pi/(5d)}^{(j+1)} | V_{Raman,j} | \psi_{q=(j-1)2\pi/(5d)}^{(j)} \rangle &= \sum_{m,m'} \frac{1}{N} e^{i \frac{2\pi}{5} [(m'-m-\frac{2}{5})j - m' + \frac{1}{5}]} \langle j+1, m | V_{Raman,j} | j, m' \rangle \\
&= \sum_m \frac{1}{N} e^{-i \frac{2\pi}{5} [m + (2j-1)\frac{1}{5}]} \langle j+1, m | V_{Raman,j} | j, m \rangle.
\end{aligned} \tag{16}$$

The intra-band terms cause a density modulation and if we only keep the near-resonant terms, the SOC Hamiltonian can be written as

$$\begin{pmatrix}
\frac{\hat{p}_2^2}{2} + \Delta_1 + \Delta_2 & c_{p,1} \frac{J}{\Delta_1} \Omega_1 e^{-i(\hat{k}_1 \cdot \hat{r} - \delta_{R,1} t)} & 0 & 0 & 0 \\
c_{p,1}^* \frac{J}{\Delta_1} \Omega_1 e^{i(\hat{k}_1 \cdot \hat{r} - \delta_{R,1} t)} & \frac{\hat{p}_2^2}{2} + \Delta_2 & c_{p,2} \frac{J}{\Delta_2} \Omega_2 e^{-i(\hat{k}_2 \cdot \hat{r} - \delta_{R,2} t)} & 0 & 0 \\
0 & c_{p,2}^* \frac{J}{\Delta_2} \Omega_2 e^{i(\hat{k}_2 \cdot \hat{r} - \delta_{R,2} t)} & \frac{\hat{p}_2^2}{2} & c_{p,3} \frac{J}{\Delta_3} \Omega_3 e^{-i(\hat{k}_3 \cdot \hat{r} - \delta_{R,3} t)} & 0 \\
0 & 0 & c_{p,3}^* \frac{J}{\Delta_3} \Omega_3 e^{i(\hat{k}_3 \cdot \hat{r} - \delta_{R,3} t)} & \frac{\hat{p}_2^2}{2} - \Delta_3 & c_{p,4} \frac{J}{\Delta_4} \Omega_4 e^{-i(\hat{k}_4 \cdot \hat{r} - \delta_{R,4} t)} \\
0 & 0 & 0 & c_{p,4}^* \frac{J}{\Delta_4} \Omega_4 e^{i(\hat{k}_4 \cdot \hat{r} - \delta_{R,4} t)} & \frac{\hat{p}_2^2}{2} - \Delta_3 - \Delta_4
\end{pmatrix},$$

where complex constants $c_{p,j}$ are the phases for each SOC terms determined by Equ. 11 and Equ. 16. We rewrite $c_{p,j} = \rho_{p,j}\theta_{p,j}$ into module parts $\rho_{p,j}$ and argument parts $\theta_{p,j}$ for later convenience. Now, to eliminate the time-dependency of spin-orbit couplings, we apply unitary transformation U_t defined as $|1\rangle_t \rightarrow |1\rangle_t e^{-i(\delta_{R,1}+\delta_{R,2})t}$, $|2\rangle_t \rightarrow |2\rangle_t e^{-i\delta_{R,2}t}$, $|3\rangle_t \rightarrow |3\rangle_t$, $|4\rangle_t \rightarrow |4\rangle_t e^{-i\delta_{R,3}t}$, $|5\rangle_t \rightarrow |5\rangle_t e^{-i(\delta_{R,3}+\delta_{R,4})t}$ for each basis $|j\rangle_t$. The Hamiltonian then turns into

$$\begin{pmatrix} \frac{\hat{p}^2}{2} & \Omega e^{-i\hat{k}_1 \cdot \hat{r}} & 0 & 0 & 0 \\ \Omega e^{i\hat{k}_1 \cdot \hat{r}} & \frac{\hat{p}^2}{2} & \Omega e^{-i\hat{k}_2 \cdot \hat{r}} & 0 & 0 \\ 0 & \Omega e^{i\hat{k}_2 \cdot \hat{r}} & \frac{\hat{p}^2}{2} & \Omega e^{-i\hat{k}_3 \cdot \hat{r}} & 0 \\ 0 & 0 & \Omega e^{i\hat{k}_3 \cdot \hat{r}} & \frac{\hat{p}^2}{2} & \Omega e^{-i\hat{k}_4 \cdot \hat{r}} \\ 0 & 0 & 0 & \Omega e^{i\hat{k}_4 \cdot \hat{r}} & \frac{\hat{p}^2}{2} \end{pmatrix},$$

where we assume that the laser strength is chosen so that each SOC terms have the same effective Raman coupling strength $\Omega = J\rho_{p,j}\Omega_j/\Delta_j$. The detunings are canceled out for exact near-resonant and the argument can always be eliminated thanks to $\theta_{p,j}\theta_{p,j}^* = 1$.

k -space configuration

For the purpose of illustration, we consider $n = 5$ case, where the effective Hamiltonian is

$$H_{5,0} = \sum_{j=1}^5 \frac{\hat{p}^2}{2} |j\rangle\langle j| + \sum_{j=1}^4 \left(\frac{\Omega}{2} e^{-2i\hat{k}_j \cdot \hat{r}} |j\rangle\langle j+1| + h.c. \right). \quad (17)$$

For each state, we apply a unitary transformation

$$|j\rangle \rightarrow e^{il_j \cdot \hat{r}} |j\rangle, \text{ for } j = 1...5, \quad (18)$$

where l_j is an undermined constant. In this new pseudo-momentum basis, l_j must satisfy the following group of equations

$$-\hat{l}_j - 2\hat{k}_j + \hat{l}_{j+1} = 0, \text{ for } j = 1...4. \quad (19)$$

to eliminate the spatial dependencies of the off-diagonal terms. However, these equations are not sufficient to determine all variables since they only contain four equations. The last one can be obtained from minimizing the single particle energy functional. Considering the simplest case $\Omega = 0$ with the kinetic energy given by

$$E_{k,0} = \frac{1}{2} \sum_{j=1}^5 \hat{l}_j^2 = \frac{1}{2} \hat{l}_1^2 + \sum_{j=2}^5 \left(\hat{l}_1 + 2 \sum_{j=1}^4 \hat{k}_j \right)^2. \quad (20)$$

Solving this functional yields $\hat{l}_1 = -\frac{2}{5} \sum_{j=1}^4 (5-j)\hat{k}_j$. Assuming we want a pentagon in momentum space with one point fixed at $(0,1)$, then the \hat{k}_j are exactly what we introduce in the main text. Inserting \hat{k}_j back to the equation we just derived, one finds $\hat{l}_1 = (0,1)$, which is consistent with our initial configuration and thus, those \hat{l}_j are nothing but the minima in k -space, that is, $\hat{l}_j = \hat{p}_j$. Note that, this is not true for arbitrary configuration but indeed holds for any regular polygon (the proof is omitted as it is straightforward). If all minima are occupied equally, we may have crystal or quasicrystal orders shown in Fig. 6. (a) is a simple crystal as it only has four minima. (b)[(c)] is quasicrystal order with five(seven)-fold rotational symmetry if one also considers the phase distribution. Note that, for any $n \geq 7$, we may expect to have quasicrystal structures in the spatial orders.

Non-zero-momentum plane-wave phase

With a finite interaction, plane-wave phase would happen at large Raman coupling situations. To evaluate the Hamiltonian at those limits, we first rewrite it in the following way

$$H'_{5,0} = \Omega \left(\frac{1}{\Omega} H_p + H_{soc} \right), \quad (21)$$

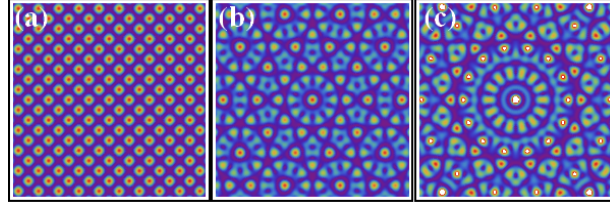


FIG. 6: (Color online) Crystalline and quasicrystal patterns in real-space when the minima in k -space form a regular polygon and all the minima are evenly populated. (a) $n = 4$, namely, a square in momentum space. This is supersolid in the context of BEC and in this case, discrete translational symmetries in both x and y directions are preserved. (b) and (c) correspond to $n = 5$ (regular pentagon) and $n = 7$ (heptagon) respectively. It is clear that now the discrete translational symmetry is broken and a corresponding rotational symmetry is presented. For (b)[(c)], it should be five(seven)-fold rotational symmetry if one considers the phase as well. Note that, any $n \geq 7$ should give a quasicrystal phase.

where $H_p = \sum_{j=1}^n \frac{1}{2}(p-p_j)^2 |j\rangle\langle j|$ is the kinetic energy and $H_{soc} = \sum_{j=1}^{n-1} (|j\rangle\langle j+1| + H.c.)$. Since Ω is large enough, we may treat the kinetic energy term as a perturbation. In this sense, the first-order correction to the energy is given by

$$E_0^{(1)} = \langle \Phi_0 | \frac{1}{\Omega} H_p | \Phi_0 \rangle = \frac{1}{2\Omega} \sum_j |a_j|^2 (p - p_j)^2, \quad (22)$$

where $\Phi_0 = \sum_j a_j |j\rangle$ is the ground state of H_{soc} with the normalization $\sum_j |a_j|^2 = 1$. Applying variation of calculus with respect to p , one finds the minimum locates at $\sum_j |a_j|^2 p_j$, which is generally not zero and thus, would give us a non-zero-momentum plane-wave phase.